

## Higher-order mode suppression in twisted single-ring hollow-core photonic crystal fibers

N. N. EDAVALATH,\* M. C. GÜNENDI, R. BERAVAT, G. K. L. WONG, M. H. FROSZ, J.-M. MÉNARD, AND P. ST.J. RUSSELL

Max Planck Institute for the Science of Light, Staudtstr. 2, 91058 Erlangen, Germany

\*Corresponding author: nitin.edavalath@mpl.mpg.de

Received 10 January 2017; revised 24 April 2017; accepted 26 April 2017; posted 3 May 2017 (Doc. ID 293271); published 17 May 2017

A hollow-core single-ring photonic crystal fiber (SR-PCF) consists of a ring of capillaries arranged around a central hollow core. Spinning the preform during drawing introduces a continuous helical twist, offering a novel means of controlling the modal properties of hollow-core SR-PCF. For example, twisting geometrically increases the effective axial propagation constant of the  $LP_{01}$ -like modes of the capillaries, providing a means of optimizing the suppression of HOMs, which occurs when the  $LP_{11}$ -like core mode phase-matches to the  $LP_{01}$ -like modes of the surrounding capillaries. (In a straight fiber, optimum suppression occurs for a capillary-to-core diameter ratio  $d/D = 0.682$ .) Twisting also introduces circular birefringence (to be studied in a future Letter) and has a remarkable effect on the transverse intensity profiles of the higher-order core modes, forcing the two-lobed  $LP_{11}$ -like mode in the untwisted fiber to become three-fold symmetric in the twisted case. These phenomena are explored by means of extensive numerical modeling, an analytical model, and a series of experiments. Prism-assisted side-coupling is used to measure the losses, refractive indices, and near-field patterns of individual fiber modes in both the straight and twisted cases. © 2017 Optical Society of America

**OCIS codes:** (060.2280) Fiber design and fabrication; (060.2430) Fibers, single-mode; (060.2310) Fiber optics; (060.2270) Fiber characterization; (060.2300) Fiber measurements; (060.5295) Photonic crystal fibers.

<https://doi.org/10.1364/OL.42.002074>

A hollow-core photonic crystal fiber (HC-PCF) has opened up a wide range of new applications for optical fibers, for example, in the delivery of high-power laser light [1], pulse compression [2], and enhanced gas-light interactions [3,4]. HC-PCFs are primarily divided into two types based on their guidance mechanism, namely, photonic bandgap and anti-resonant reflection (ARR) [5]. A common example of an ARR-PCF is kagomé-PCF [6], which offers relatively low transmission loss over broad spectral ranges in the visible and near-infrared. Stacking a kagomé-PCF preform requires a large number of

capillaries, but renders the production cumbersome and time-consuming. In addition, optical resonances in the many struts and junctions in the extended kagomé-PCF cladding phase-match to the core mode at certain wavelengths, giving rise to loss peaks that degrade the flatness of the transmission spectrum.

Recently, simpler ARR-PCF structures have been introduced in which the number of cladding unit cells is reduced to a single ring of capillaries surrounding the core [Fig. 1(a)] [7–10]. These capillaries are designed as anti-resonant elements that block leakage of the  $LP_{01}$ -like core mode [10,11]. Impressively low losses can be reached with these very simple structures [9].

Although an SR-PCF is easier to fabricate than the structurally more complex kagomé-PCF, and does not suffer from a multiplicity of cladding resonances, it generally supports several HOMs with losses that are often comparable to those of the  $LP_{01}$ -like core mode. This makes it difficult to launch a pure fundamental mode, as required in many applications. Several recent studies have tried to address this issue using a range of different approaches.

One such technique is based on phase-matching the  $LP_{11}$ -like core mode to the  $LP_{01}$ -like modes of the capillaries,

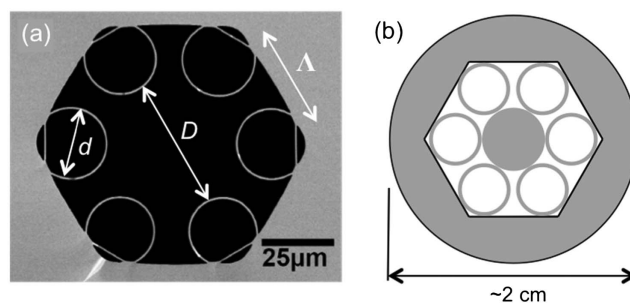


**Fig. 1.** (a) Scanning electron micrograph of an SR-PCF with a core diameter  $D = 44 \mu\text{m}$ , a capillary diameter  $d = 23 \mu\text{m}$ , and a capillary wall thickness  $t = 0.7 \mu\text{m}$ . The inter-capillary distance  $\Lambda = (D + d)/2$ . (b) Schematic of the initial silica SR-PCF stack, consisting of a jacket tube with a hexagonal inner bore and six capillaries held in place at the vertices by a central glass rod inserted at each end of the stack.

thus providing a leakage channel for HOMs. Optimum HOM suppression for hollow core fibers turns out to occur at  $d/D = 0.682$ , where  $d$  is the inner diameter of the capillaries, and  $D$  is the core diameter [12]. The fabrication tolerances for reaching this condition, however, are very stringent—often the capillaries end up being too small. It is also important to suppress phase-matching to resonances in the capillary walls, which give rise to bands of high loss in the transmission spectrum. The fundamental (longest wavelength) band occurs at  $\lambda_0 = 2b(n_g^2 - 1)^{0.5}$ , where  $n_g$  is the refractive index of the glass ( $\sim 1.46$ ), and  $b$  is the wall thickness. For example, if it is desired to guide light down to 400 nm,  $b$  must be thinner than 188 nm. The requirement for very thin capillary walls makes it even more challenging to reach  $d/D = 0.682$ . When  $d/D$  is sub-optimal, the modal refractive index of the LP<sub>11</sub>-like core mode is higher than the index of the LP<sub>01</sub>-like capillary modes.

Here we report that this difficulty can be overcome by introducing a helical twist, with a precise pitch, during the drawing process. A similar procedure has been used to strip off HOMs in solid-core fibers, using one or more satellite cores that spiral around a straight central core, rendering the core effectively single mode [13]. For an off-axis field lobe that is forced by the microstructure to follow a spiral path, twisting has the effect of geometrically increasing its effective path length (and, thus, its modal index) along the fiber axis by a factor  $(1 + \alpha^2 \rho^2)^{0.5}$ , where  $\alpha = 2\pi/L$  is the twist rate,  $L$  is the helical pitch, and  $\rho$  is the distance from the fiber axis [14,15]. As a result, the index of the capillary modes is increased by a factor  $(1 + \alpha^2(d + D)^2/4)^{0.5}$  and that of the LP<sub>11</sub>-like core mode by a factor  $(1 + \alpha^2 \rho_L^2)^{0.5}$ , where  $\rho_L = \gamma D$  is the radial position of the lobes, and  $\gamma$  is a numerical factor (see below).

In addition, because its individual field lobes are strongly coupled to each other, the LP<sub>11</sub>-like core mode will transform into a helical Bloch mode in the twisted fiber, with azimuthal harmonics of the orbital angular momentum (OAM) order  $\ell^{(m)} = \ell_0 + mN$ , where  $\ell_0$  is the order of the principal (strongest) harmonic,  $m$  is the harmonic order, and  $N$  is the number of field lobes [16]. The  $m$ th harmonic will have an axial refractive index greater by an amount  $\ell^{(m)}\alpha\lambda/2\pi$  than in the straight fiber. (This does not occur in the ring of capillaries because they are only very weakly coupled, if at all.)

Combining all these effects yields a condition at which the indices of the higher-order core mode and capillary mode match:

$$n_{01}\sqrt{1 + \alpha^2(d + D)^2/4} = \ell^{(m)}\alpha\lambda/(2\pi) + n_{11}\sqrt{1 + \alpha^2\gamma^2 D^2}, \quad (1)$$

where

$$n_{01} = \sqrt{1 - (u_{01}\lambda/(\pi f_{01}d))^2} \quad \text{and} \\ n_{11} = \sqrt{1 - (u_{11}\lambda/(\pi f_{11}D))^2}, \quad (2)$$

are the modal indices of the LP<sub>01</sub> and LP<sub>11</sub> modes in a straight capillary, and  $u_{kl}$  is the  $l$ th zero of a Bessel function of order  $k$  and the correction factors  $f_{11} = 1.077$  and  $f_{01} = 0.991$  (these values remain valid for all the  $d/D$  values reported in this Letter) [12,17]. Recognizing that the second terms under the square-roots are all much less than unity, and taking terms up to the first order, Eq. (1) can be re-cast in the form

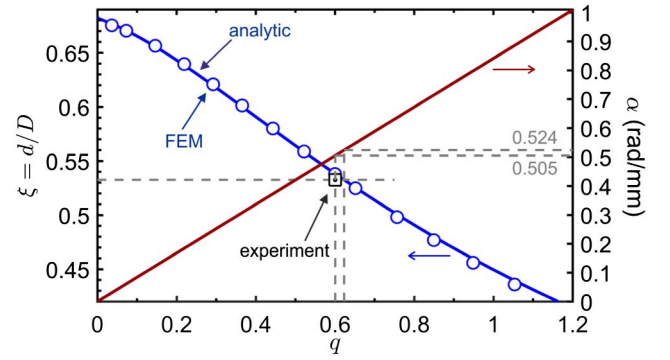


**Fig. 2.** Left-hand axis: the value of  $\xi = d/D$  that provides optimal HOM suppression, plotted against the parameter  $q$  (see the text). The open circles are FEM calculations, and the full curve is a solution of Eq. (3). The agreement is excellent. Right-hand axis:  $\alpha$  plotted against  $q$  for the experimental parameters. The dot surrounded by a square corresponds to the experimental value  $\xi = 0.533$ , showing that the experimental twist rate (0.505 rad/mm) lies quite close to the optimal value of 0.524 rad/mm for this value of  $\xi$ .

$$q^2 - q \left( \frac{2f_{01}\ell^{(m)}}{u_{01}((\xi + 1)^2 - 4\gamma^2)} \right) - \left( \frac{\xi_0^2 - \xi^2}{\xi^2 \xi_0^2 ((\xi + 1)^2 - 4\gamma^2)} \right) = 0, \quad (3)$$

where

$$q = \pi \alpha f_{01} D^2 / (2\lambda u_{01}), \quad (4)$$

and  $\xi_0 = u_{01}f_{11}/(u_{11}f_{01})$  is the optimal value of  $\xi = d/D$  at a zero twist rate.

Figure 2 plots the positive-valued solution of Eq. (3), together with the results of finite element modeling for a structure with six identical circular capillaries placed 60° apart ( $d/D = 0.533$ ,  $D/\lambda = 41.6$ , capillary wall thickness  $t = 700$  nm). Excellent agreement is obtained for  $\gamma = 0.175$  and  $\ell^{(m)} = -1$ , i.e., for the lowest index Bloch harmonic that has an appreciable amplitude. The optimum twist rate for the experimental parameters ( $\lambda = 1064$  nm and  $D = 44$  μm) is 0.524 rad/mm, as shown on the right-hand axis.

Armed with this analytical model as a guide, we carried out a series of experiments and numerical simulations, comparing the properties of the modes in the twisted and untwisted versions of the same single-ring HC-PCF structure.

The fibers were fabricated using a modified version of the two-step stack-and-draw technique. The structure was first stacked by placing capillaries at the vertices of a jacket tube with a hexagonal inner profile and holding them in place by two central support rods, one at each end of the stack [Fig. 1(b)]. This structure was first drawn down to an intermediate cane of outer diameter  $\sim 2$  mm, which was then spun around its axis while being drawn down to the fiber [16]. The twist rate is set by the drawing and rotation speeds, and long lengths (limited only by size of the cane) of a twisted single-ring HC-PCF could be drawn with minimal structural distortion. Twisted and untwisted SR-PCFs were drawn with the structural parameters listed in Fig. 1, yielding  $d/D = 0.533$ , which is sub-optimal for HOM suppression in the an untwisted fiber at 1064 nm. The twisted fiber had  $\alpha = 0.505$  rad/mm, which is within 4% of the optimum value for HOM suppression

(0.514 rad/mm). With further technical development, it should be possible to hit the exact twist rate by precisely measuring  $d/D$  during drawing and adjusting the rotation rate accordingly.

The fiber modes were characterized using prism-assisted side-coupling, which allows light to be fed precisely into a selected individual fiber mode, provided it is leaky enough [18]. The effective modal refractive indices, losses, and associated modal patterns of the HOMs can then be studied in detail. The experiment involves placing a wedge prism (face slanted at  $1.1^\circ$ ) on the side of the SR-PCF with a layer of index-matching fluid in between. Light from a 1064 nm diode laser was coupled into a commercially available single-mode fiber (SMF), the output of which was collimated to a full-width at half-maximum beam width of 2 mm. This beam was then arranged to be incident on the slanted face of the wedge prism, at an angle  $\psi$  to its face normal, and focused on a line parallel to the fiber axis using a cylindrical lens (focal length of 30 mm). The SMF and the lens were mounted together on a rotation stage so as to allow  $\psi$  to be precisely varied.

As  $\psi$  is increased, successive HOMs are excited when the wavevector component along the fiber axis matches the wavevector of a mode. The near-field intensity profiles of the modes can then be imaged at the fiber end using a CCD camera. Unlike end-fire coupling, where precise matching of the modal profile is essential if excitation of unwanted modes is to be avoided, prism-assisted side-coupling allows pure HOMs to be selectively excited without prior knowledge of their field profile. Once a mode is optimally excited, its modal refractive index can be calculated [18] from the measured beam angle, taking careful account of refractive indices at 1064 nm (1.4496 for the silica glass prism at 1064 nm and 1.0003 for air). The procedure is then repeated for different fiber lengths, allowing the loss of each mode to be evaluated with good accuracy.

Figure 3 plots the measured propagation losses and modal refractive indices of the modes in the twisted and untwisted SR-PCF, and the corresponding near-field mode profiles are shown in Figs. 4(a) and 4(b). In the untwisted case, it is fairly

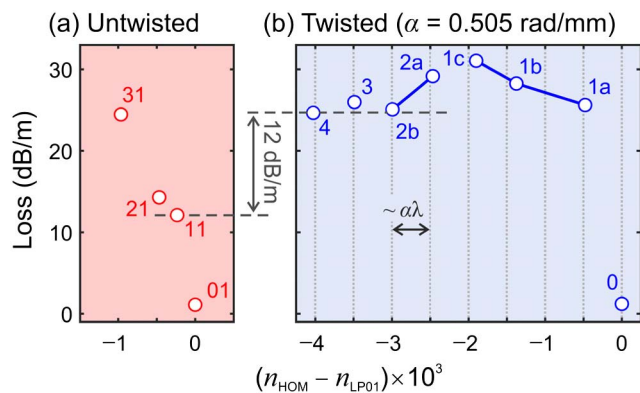


**Fig. 3.** HOM losses, measured using prism coupling, plotted versus a modal refractive index for an SR-PCF with  $d/D = 0.533$ . (a) Untwisted case; the labels next to the data-points (red circles) indicate the azimuthal  $k$  and radial  $l$  orders of the  $LP_{kl}$ -like modes. (b) At a twist rate of 0.505 rad/mm. Modes with similar near-field distributions (see Fig. 4) are grouped together. The spacing between successive modes is approximately equal to a multiple of  $a\lambda$  (see the text). The loss of HOMs is increased by at least 12 dB/m in the twisted fiber.

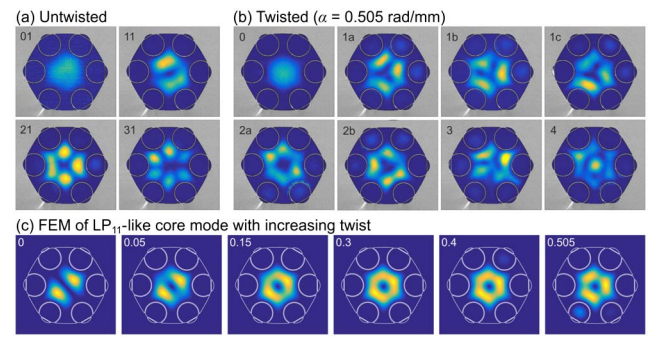


**Fig. 4.** (a) and (b) Measured optical near-field distributions of modes excited by prism-assisted side-coupling at 1064 nm in 60 cm lengths of (a) an untwisted and (b) a twisted ( $\alpha = 0.505$  rad/mm) SR-PCF. The mode profiles are superimposed on a scanning electron micrograph of the fiber structure. The corresponding modal losses and refractive indices are plotted in Fig. 3. (c) Numerically modeled Poynting vector distributions showing how the double-lobed  $LP_{11}$ -like mode of the untwisted fiber evolves into a triple-lobed pattern in the twisted fiber as the twist rate increases. (The values correspond to rad/mm.) The structural parameters are  $d/D = 0.533$ ,  $D/\lambda = 41.6$ , and  $t = 700$  nm.

straightforward to identify the modes and label them using the  $LP_{kl}$  notation, where  $k$  and  $l$  are the azimuthal and radial orders, respectively [Figs. 3(a) and 4(a)].

In the twisted case, however, it is more difficult to identify the HOMs using the LP notation, because they are strongly affected by the twist. Nevertheless, it is possible to arrange them in groups with similar-looking field profiles, as is done in Fig. 4(b). Group 1 (containing 1a, 1b, and 1c) modes have three-fold symmetry, whereas Group 2 (2a and 2b) modes have six-fold symmetry. Mode 3 is somewhat difficult to identify, but mode 4 clearly has some similarity with an  $LP_{32}$  mode.

The evolution of the modal Poynting vector distribution of the first HOM [Group 1 in Fig. 3(b)] with an increasing twist rate is explored numerically in Fig. 4(c). It evolves from a double-lobed pattern through a doughnut shape at 0.150 rad/mm to a triple-lobed pattern at 0.505 rad/mm. The fundamental  $LP_{01}$ -like mode remains unaffected.

To understand the results in Fig. 3(b), it is necessary first to realize that the both axial and azimuthal phase-matching must be satisfied for prism coupling to work. The additional azimuthal component of momentum comes from the slanted capillaries, which act as a long-period grating (Fig. 5). The azimuthal component of the refractive index at point P can be written in the form

$$n_{az}^m = \frac{m\lambda}{\Lambda} \cos \theta - n_{\text{prism}} \sin \phi \simeq \frac{m\lambda}{\Lambda} - n_{\text{prism}} \sin \phi, \quad (5)$$

where  $m$  is the diffracted order,  $n_{\text{prism}}$  the index set by the prism,  $\theta \simeq \alpha\lambda$  is the slant angle of the capillaries, and  $\phi$  is a possible angular deviation of the incident rays from the fiber axis, caused by prism misalignment or the angular spread of the incident beam. In order to excite an OAM mode of order  $\ell$ ,  $m$  and  $\phi$  must satisfy the equation  $\ell = N\Lambda'[(n_{\text{prism}}/\lambda) \sin \phi + m/\Lambda]$ , where  $\Lambda'$  is the distance between the adjacent field lobes of a core mode with  $N$ -fold rotational symmetry, i.e.,  $N\Lambda' \simeq 2\pi\gamma D$ . The axial refractive index component of the mode is then given by

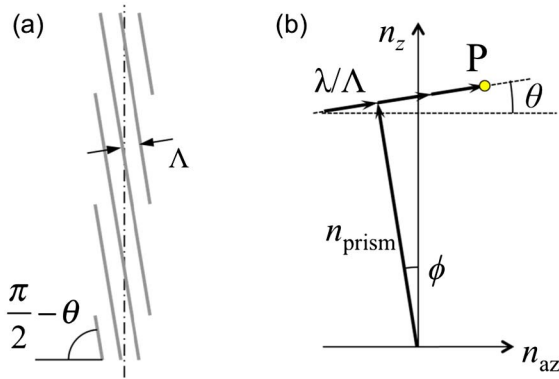


**Fig. 5.** (a) Top view of the capillaries, spaced by  $\Lambda = (D + d)/2$  and slanted at angle  $\phi \approx \alpha\Lambda$  to the fiber axis. (b) Refractive index diagram of the grating. The axial component of refractive index at P is  $n_z \approx n_{\text{prism}} + m\alpha\lambda$  (see the text).

$$n_z \approx n_{\text{prism}} + m\alpha\lambda, \quad (6)$$

where the approximation  $\cos \phi \approx 1$  has been used. This equation shows that the modal index measured by the prism will be smaller than its actual value by  $m\alpha\lambda$ , where  $m$  increases by approximately 1 for modes with a successively higher OAM order. (Note that the negative values of  $m$  which, in our definition, imply higher values of the axial index, are unlikely to result in excitation of a mode because there is less field penetration outside the core, making prism coupling much less efficient.)

The predictions of Eq. (6) are confirmed by the measurements in Fig. 3(b), where the index spacing between successive modes corresponds approximately to multiples of  $\alpha\lambda = 5.3 \times 10^{-4}$ . Between modes 1a and 1b, the index measured by the prism falls by roughly twice this amount, which we tentatively attribute to uncertainties in the angle  $\phi$ .

Although all of the HOMs experience higher loss in the twisted fiber, for pure single-mode operation it is most important that the LP<sub>11</sub>-like mode is strongly suppressed, since it is the one most easily excited by end-fire coupling. Comparing the twisted and untwisted cases (Fig. 3), it is clear that the LP<sub>11</sub> mode is indeed strongly suppressed by twisting. While the measured loss of the fundamental mode is practically unaffected by the twist (1.1 dB/m [untwisted] versus 1.2 dB/m [twisted]), the overall HOM loss increase is >12 dB/m. The calculated losses for the LP<sub>01</sub> and LP<sub>11</sub> modes in the untwisted case are 1.0 and 2.8 dB/m, respectively.

In Fig. 6, the calculated wavelength dependence of the figure-of-merit for LP<sub>11</sub>-like mode suppression, defined as  $\text{FOM}_{11} = (\alpha_{11} - \alpha_{01})/(\alpha_{11} + \alpha_{01})$ , is plotted. ( $\text{FOM}_{11} = 1$  indicates perfect LP<sub>11</sub>-like mode suppression.) There is good agreement between the predicted ( $\sim 0.87$ ) and measured (0.91) values of  $\text{FOM}_{11}$ , even though the experimental error in measuring the fundamental mode loss is quite high, since the loss is so low, and the fiber length is short.

In conclusion, twisting provides a novel additional design tool for manipulating the modal properties of SR-PCFs. It induces a geometrical increase in path length for the capillary modes, making it possible to phase-match them to an LP<sub>11</sub>-like core mode, even when the  $d/D$  value is sub-optimal, rendering the fiber effectively single-mode. By appropriate design

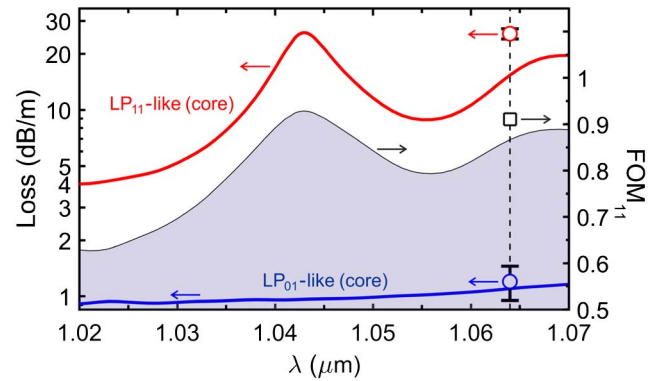


**Fig. 6.** Wavelength dependence of the loss (left-hand axis) for the LP<sub>01</sub>-like core and capillary modes, and the LP<sub>11</sub>-like core mode, calculated by FEM for the actual fiber structure, including variations in the diameter and position of each capillary, for a twist rate of 0.505 rad/mm. The corresponding theoretical figure-of-merit for suppression of the LP<sub>11</sub> mode,  $\text{FOM}_{11}$  (see the text), is the under-shaded curve. The experimental values of loss at 1064 nm are marked with circles, and the corresponding  $\text{FOM}_{11}$  is marked by a square.

(for example, by arranging that  $d/D > 0.682$  or by achieving higher twist rates), it should be possible to suppress the fundamental mode by twisting, while maintaining a low loss LP<sub>11</sub>-like mode.

**Funding.** Max-Planck-Gesellschaft (MPG).

## REFERENCES

- P. Jaworski, F. Yu, R. R. J. Maier, W. J. Wadsworth, J. C. Knight, J. D. Shephard, and D. P. Hand, *Opt. Express* **21**, 22742 (2013).
- K. F. Mak, J. C. Travers, N. Y. Joly, A. Abdolvand, and P. St.J. Russell, *Opt. Lett.* **38**, 3592 (2013).
- J. C. Travers, W. Chang, J. Nold, N. Y. Joly, and P. St.J. Russell, *J. Opt. Soc. Am. B* **28**, A11 (2011).
- P. St.J. Russell, P. Hölzer, W. Chang, A. Abdolvand, and J. C. Travers, *Nat. Photonics* **8**, 278 (2014).
- N. M. Litchinitser, S. C. Dunn, B. Usner, B. J. Eggleton, T. P. White, R. C. McPhedran, and C. M. de Sterke, *Opt. Express* **11**, 1243 (2003).
- F. Benabid and P. J. Roberts, *J. Mod. Opt.* **58**, 87 (2011).
- F. Gérôme, R. Jamier, J.-L. Auguste, G. Humbert, and J.-M. Blondy, *Opt. Lett.* **35**, 1157 (2010).
- A. D. Pryamikov, A. S. Biriukov, A. F. Kosolapov, V. G. Plotnichenko, S. L. Semjonov, and E. M. Dianov, *Opt. Express* **19**, 1441 (2011).
- F. Yu, W. J. Wadsworth, and J. C. Knight, *Opt. Express* **20**, 11153 (2012).
- S. Février, B. Beaudou, and P. Viale, *Opt. Express* **18**, 5142 (2010).
- M. Alharbi, T. Bradley, B. Debord, C. Fourcade-Dutin, D. Ghosh, L. Vincetti, F. Gérôme, and F. Benabid, *Opt. Express* **21**, 28609 (2013).
- P. Uebel, M. C. Günendi, M. H. Frosz, G. Ahmed, N. N. Edavalath, J.-M. Ménard, and P. St.J. Russell, *Opt. Lett.* **41**, 1961 (2016).
- X. Ma, C. Zhu, I.-N. Hu, A. Kaplan, and A. Galvanauskas, *Opt. Express* **22**, 9206 (2014).
- R. Beravat, G. K. L. Wong, M. H. Frosz, X. M. Xi, and P. St.J. Russell, *Sci. Adv.* **2**, e1601421 (2016).
- P. St.J. Russell, R. Beravat, and G. K. L. Wong, *Phil. Trans. R. Soc. A* **375**, 20150440 (2017).
- X. M. Xi, G. K. L. Wong, M. H. Frosz, F. Babic, G. Ahmed, X. Jiang, T. G. Euser, and P. St.J. Russell, *Optica* **1**, 165 (2014).
- M. A. Finger, N. Y. Joly, T. Weiss, and P. St.J. Russell, *Opt. Lett.* **39**, 821 (2014).
- B. M. Trabold, D. Novoa, A. Abdolvand, and P. St.J. Russell, *Opt. Lett.* **39**, 3736 (2014).